

Quantum Revivals of Morse Oscillators and Farey-Ford Geometry

Alvason Zhenhua Li* and William G. Harter†
Microelectronics-Photonics Program, Department of Physics,
University of Arkansas, Fayetteville, AR 72701, USA
 (Dated: May 29, 2013)

Analytical eigensolutions for Morse oscillators are used to investigate quantum resonance and revivals and show how Morse anharmonicity affects revival times. A minimum semi-classical Morse revival time $T_{min-rev}$ found by Heller is related to a complete quantum revival time T_{rev} using a quantum deviation δ_N parameter that in turn relates T_{rev} to the maximum quantum beat period $T_{max-beat}$. Also, number theory of Farey and Thales-circle geometry of Ford is shown to elegantly analyze and display fractional revivals. Such quantum dynamical analysis may have applications for spectroscopy or quantum information processing and computing.

PACS numbers: 03.65.-w, 34.10.+x, 82.53.-k

Wavepacket dynamics has a long history that has more recently been accelerated by graphics that exhibit space-time behavior. Such studies began with revivals in cavity QED simulations by Eberly [1] and later simulations of molecular rovibronic dynamics [2, 3]. Ultrafast laser spectroscopy made it possible to observe wavepacket resonance and localized periodic motion in experimental situations [4–6] involving AMOP dynamics [6, 7]. This helped reveal new physics and chemistry of ultrafast spectroscopy [7, 8].

Some of this involves symmetry and number theoretic properties of wavepacket space-time structure, a still largely unexplored field. The following development is based upon earlier Cn -group and Farey-sum-tree [9] analysis of quantum rotors [10, 11] as cited by Schleich et al. [12, 13] for possible numeric factorizing applications. That work treated only R(2) rings or 1D infinite-wells but nevertheless revealed general symmetry properties.

Here Morse oscillators are shown to share Farey-sum revival structure of R(2) rings or 1D infinite-wells. Moreover, Morse revivals reveal concise ways to find complete revival times T_{rev} along with new ways to quantify quantum wavepacket dynamics using Ford circles [14][15].

The Morse oscillator potential (Eq. (1a)) is an anharmonic potential [16] used to describe covalent molecular bonding. Some dynamics of Morse states have been studied [17–21] as a model of vibrational anharmonicity.

$$V_M(x) = D(1 - e^{-\alpha x})^2 \quad (1a)$$

Coordinate x is variation of bond from equilibrium where the potential has its minimum and zero value at $x = 0$. Coefficient D is bond dissociation energy and its maximum inflection value at infinite x . D relates harmonic frequency ω_e in Eq. (1b) and anharmonic frequency ω_χ in Eq. (1c) that gives width parameter α . The latter is related to reduced mass μ and anharmonic frequency ω_χ .

$$D = \frac{\omega_e^2}{4\omega_\chi} \hbar \quad (1b)$$

$$\alpha = \sqrt{\frac{2\omega_\chi\mu}{\hbar}} = \sqrt{\frac{\omega_e^2\mu}{2D}} \quad (1c)$$

McCoy [22] revived interest in exact eigenfunctions and eigenvalues [23] of Morse oscillator used in Eqs. (2) and (3a) below and allows analysis of its quantum dynamics that may be relevant to anharmonic dynamics in general.

The Morse oscillator, being anharmonic, has varying spacing of its energy levels in contrast to uniform (harmonic) spacing. At high quanta n , energy levels $E_n = \hbar\omega_n$ have low- n spacing $\Delta E = \hbar\omega_e$ compressed for positive anharmonic frequency ω_χ in Eq. (2).

$$E_n = \hbar\omega_n = \hbar\omega_e(n + \frac{1}{2}) - \hbar\omega_\chi(n + \frac{1}{2})^2 \quad (2)$$

The corresponding Morse eigenfunctions of the eigenvalues are given by Eq. (3a) where L_n^{2s} represents a generalized associated Laguerre polynomial [22].

$$\phi_n(x) = e^{-\frac{y(x)}{2}} y(x)^{s(n)} \sqrt{\frac{\alpha(\nu - 2n - 1)n!}{\Gamma(\nu - n)}} L_n^{2s(n)}(y(x)) \quad (3a)$$

Exponentially scaled $y(x)$ has exponent $s(n)$ as given.

$$y(x) = \nu e^{-\alpha x} \quad (3b)$$

$$s(n) = \frac{1}{2}(\nu - 2n - 1) \quad (3c)$$

The scaling parameter ν is as follows.

$$\nu = \frac{4D}{\hbar\omega_e} \quad (3d)$$

Dynamic waves are combinations of eigenfunctions.

$$\psi(x, t) = \sum_{n=0}^{n_{max}} c_n \phi_n(x) e^{-i\frac{E_n t}{\hbar}} \quad (4)$$

Here n_{max} is the highest bound state. Its eigenvalue is nearest to dissociative limit D . To get maximum beating

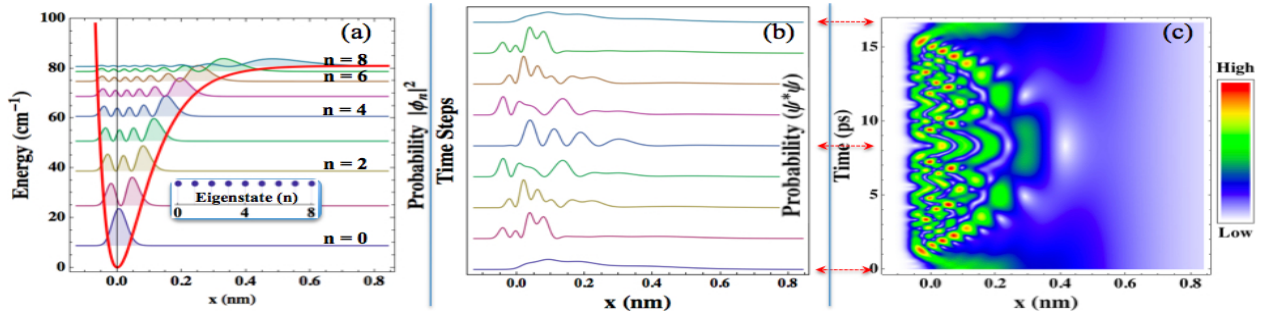


FIG. 1. The Morse oscillator with a harmonic frequency $\omega_e/2\pi c = 18(\text{cm}^{-1})$ and an anharmonic frequency $\omega_\chi/2\pi c = 1(\text{cm}^{-1})$. (a) Each of its stationary eigenstate $|\phi_n|^2$ was list-plotted on a energy level of eigenvalue E_n in the potential well (red-color-line), these wave functions are normalized (indicated by the same-height dotted-line). (b) The wave packet $\psi^*\psi$ is propagated along the time steps. (c) The probability density map of the wave packet $|\psi|^2$ as a function of space and time. The double arrows connecting (b)-(c) indicate the corresponding time events.

we assume equal Fourier coefficients $c_n = 1$. (We do not consider shorter revivals had by zeroing select c_n .)

A sample Morse oscillator potential shown in Fig. 1(a) has a total of nine stationary bound states (from $n = 0$ to $n_{max} = 8$). The initial wave packet (Eq. (4) at $t = 0$) is a sum of these stationary bound states and evolves as shown in Fig. 1(b) ending in its lowest $\psi(x, T)^*\psi(x, T)$ trace as the initial shape fully revived.

Space-time plots of the norm $|\psi(x, t)|$ in Fig. 1 (c) show resonant beat nodes and anti-nodes that outline semi-classical trajectories $x(t)$ corresponding to energy values E_n ranging from the lowest ground state E_0 up to the highest bound state $E_{n_{max}}$.

An essential part of wave packet dynamics analysis of anharmonic systems is to predict if and when exact wave packet revival might occur. If T_{rev} is a time for a Morse oscillator revival, then Wang and Heller [21] have shown

$$T_{rev} = \frac{\pi}{\omega_\chi} \mathbb{M} \quad (5a)$$

where \mathbb{M} is an integer. This revealed two facts about Morse oscillator dynamics. First, there may be minimum or fundamental revival period at

$$T_{min-rev} = \frac{\pi}{\omega_\chi} \quad (5b)$$

This is the shortest revival time for Morse oscillator found by Wang and Heller [21]. Second, any complete revival period is made of integer numbers of the fundamental period. That is, any complete quantum revival must contain integer numbers of semiclassical-trajectory-profile periods (minimum revival period) which is approximately outlined by a classical particle oscillating with a frequency of $2\omega_\chi$ in the Morse potential.

To illustrate relations between quantum periods and semiclassical-trajectory-profile periods, consider three cases of classical particles with corresponding quantum eigenvalue energies orbiting in a Morse potential as shown

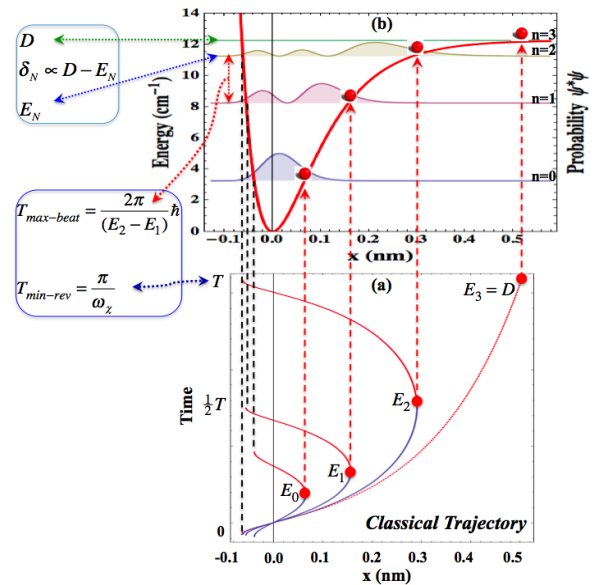


FIG. 2. Relating the maximum beat period and semiclassical-trajectory-profile period (the minimum revival period). (a) 3 classical trajectories of particles oscillating in a Morse potential are plotted in one period time, and one additional classical trajectory of particle with dissociation energy D is also plotted. The red-dots in (a) and (b) indicate that these classical particles have the same energies as the corresponding quantum eigenvalue energies. (b) The probability amplitudes of 3 bound quantum eigenfunctions are listed along energy level in a Morse potential (red-thick-line).

Fig. 2 (a). Here the rainbow-shape trajectory of a classical particle with energy E_2 has a classical oscillating period T close to the fundamental period of π/ω_χ , while a classical trajectory with energy $E_3 = D$ is of a particle barely escaping from its Morse potential well.

The preceding case has a simple revival period formula. More analysis is required to determine a specific integer \mathbb{M} of Eq. (5a) for Morse revivals for a given (ω_e, ω_χ) .

Beating of waves with nearby frequency plays a key

role in quantum dynamics. The maximum beat period $T_{max-beat}$ due to the closest bound energy level pair in the Morse well is one key to finding its revival period. A complete revival of $|\Psi(x, t)|^2$ at time T_{rev} must contain integer numbers of all beat periods including at least one fundamental time period $T_{max-beat}$ for the slowest beat frequency. This relates it to revival period.

$$T_{rev} = T_{max-beat}\mathbb{N} \quad (6)$$

Here \mathbb{N} is an integer. The Morse energy level Eq. (2) gives a beat-gap between neighboring energy.

$$\Delta E = E_n - E_{n-1} = \hbar(\omega_e - 2\omega_\chi n) \quad (7)$$

The ΔE is the minimum for maximum n occurring between the highest bound quantum numbers n_{max} and n_{max-1} . Planck's relation $E = \hbar\omega$ gives maximum beat period.

$$\begin{aligned} T_{max-beat} &= \frac{2\pi}{(\Delta\omega)_{min}} = \frac{2\pi}{E_{n_{max}} - E_{n_{max-1}}} \hbar \\ &= \frac{2\pi}{\omega_e - 2\omega_\chi n_{max}} \end{aligned} \quad (8)$$

To estimate upper bound quantum n_{max} in Eq. (8), we suppose n_{max} is the integer part of a real number n_{real} and substitute n_{real} into energy Eq. (2) to give $E_{n_{real}}$ that equals dissociative limit D in Eq. (1b). This equivalent relation is expressed as

$$\begin{aligned} E_{n_{real}} &= \hbar\omega_e(n_{real} + \frac{1}{2}) - \hbar\omega_\chi(n_{real} + \frac{1}{2})^2 \\ &= D = \frac{\omega_e^2}{4\omega_\chi} \hbar \end{aligned} \quad (9a)$$

A perfect square equation gives one root.

$$n_{real} = \frac{\omega_e}{2\omega_\chi} - \frac{1}{2} \quad (9b)$$

The integer part or floor of n_{real} is the highest Morse quantum number n_{max} (For Fig. 1, this is $n_{max} = 8$).

$$n_{max} = \text{Floor}[n_{real}] = \text{Floor}[\frac{\omega_e}{2\omega_\chi} - \frac{1}{2}] \quad (9c)$$

The fractional part δ_N of n_{real} is quantum defect of dissociative level D and highest allowed bound energy level.

$$\delta_N = n_{real} - n_{max} \quad (9d)$$

As illustrated in Fig. 2(b), δ_N is proportional to energy gap between D and the highest bound energy level.

Then, the fundamental period $T_{max-beat}$ in Eq. (8) is expressed in term of δ_N .

$$\begin{aligned} T_{max-beat} &= \frac{2\pi}{\omega_e - 2\omega_\chi n_{max}} = \frac{2\pi}{\omega_e - 2\omega_\chi(n_{real} - \delta_N)} \\ &= \frac{2\pi}{\omega_e - 2\omega_\chi(\frac{\omega_e}{2\omega_\chi} - \frac{1}{2} - \delta_N)} \\ &= \frac{\pi}{\omega_\chi(\delta_N + \frac{1}{2})} \end{aligned} \quad (10a)$$

Eq. (10a) is rewritten by substituting $T_{min-rev} = \pi/\omega_\chi$ given by Eq. (5b).

$$T_{max-beat} = \frac{\pi}{\omega_\chi(\delta_N + \frac{1}{2})} = T_{min-rev} \frac{1}{(\delta_N + \frac{1}{2})} \quad (10b)$$

This relates two fundamental building blocks of a complete Morse revival period.

$$\frac{T_{min-rev}}{T_{max-beat}} = \delta_N + \frac{1}{2} \quad (11a)$$

As discussed for Eqs. (5a) and (6), a perfect quantum revival period of the Morse oscillator T_{rev} is composed of integer numbers of the fundamental periods as follows.

$$T_{rev} = T_{min-rev}\mathbb{M} = T_{max-beat}\mathbb{N} \quad (11b)$$

Then Eqs. (11a) and (11b) relate \mathbb{N} and \mathbb{M} integers.

$$\frac{\mathbb{N}}{\mathbb{M}} = \delta_N + \frac{1}{2} \quad (11c)$$

The quantum beat-period approach gives Morse revival time T_{rev} in terms of $T_{max-beat}$ and δ_N as follows.

$$T_{rev} = T_{max-beat}\mathbb{N} = T_{max-beat} \text{Numerator}[\delta_N + \frac{1}{2}] \quad (12a)$$

The semiclassical-trajectory-profile approach gives T_{rev} in terms of $T_{min-rev}$ and δ_N as follows.

$$T_{rev} = T_{min-rev}\mathbb{M} = T_{min-rev} \text{Denominator}[\delta_N + \frac{1}{2}] \quad (12b)$$

Both $T_{min-rev}$ or $T_{max-beat}$ serve as a fundamental building blocks of T_{rev} . Examples of this follow.

Interplay of harmonicity and anharmonicity of Morse oscillators affects revival period T_{rev} . Consider Fig. 3 (a)-(c) where the value of T_{rev} is increased from the minimum revival period $T_{min-rev}$ to multiples thereof with fixed anharmonic frequency $\omega_\chi/2\pi c = 1(\text{cm}^{-1})$.

In Fig. 3(a) with $\omega_e/2\pi c = 18(\text{cm}^{-1})$ one perfect revival occurs in the minimum revival time: $T_{rev} = T_{max-beat} = T_{min-rev}$ giving a unit ratio $T_{min-rev}/T_{max-beat} = 1/1$.

Then in Fig. 3(b) with $\omega_e/2\pi c = 17(\text{cm}^{-1})$ and the same ω_χ , is seen a double time for perfect revival of $T_{rev} = T_{max-beat} = 2T_{min-rev}$ with a half ratio $T_{min-rev}/T_{max-beat} = 1/2$. We note that this double revival time $T_{rev} = 2T_{min-rev} = 2\pi/\omega_\chi$ exactly equals T_{approx} in Eq. (13) given by a semiclassical treatment of general anharmonic oscillators [24-27] that assumes large quantum numbers n around their average \bar{n} .

$$T_{approx} = \frac{2\pi}{\frac{1}{2} \left| \frac{d^2 E_n}{dn^2} \right|_{n=\bar{n}}} = \frac{2\pi}{\omega_\chi} \quad (13)$$

In Fig. 3(c) with $\omega_e/2\pi c = 17 + \frac{1}{3}(\text{cm}^{-1})$ is a perfect revival time $T_{rev} = 2T_{max-beat} = 3T_{min-rev}$ with ratio

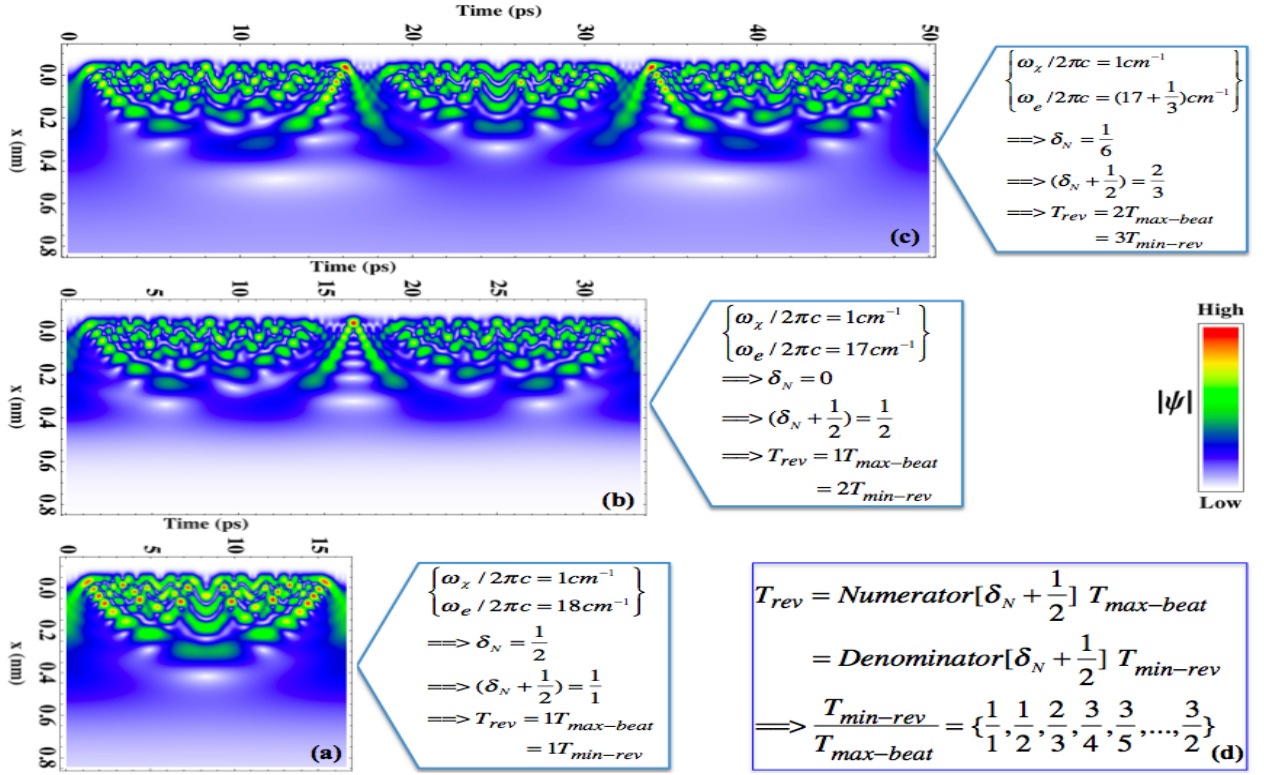


FIG. 3. Fibonacci sequence and exchange rate. (a) When $\delta_N = 1/2$, the T_{rev} is composed of one $T_{max-beat}$ and one $T_{min-rev}$. (b) When $\delta_N = 0$, the T_{rev} is composed of $1T_{max-beat}$ and $2T_{min-rev}$. (c) When $\delta_N = 1/6$, the T_{rev} is composed of $2T_{max-beat}$ and $3T_{min-rev}$. (d) Allowed ratios of $T_{min-rev}$ to $T_{max-beat}$.

of minimum revival period to maximum beat period of $T_{min-rev}/T_{max-beat} = 2/3$.

All revival periods T_{rev} are composed of an integer number of fundamental period $T_{min-rev}$ (or $T_{max-beat}$) but have a differing ratios $T_{min-rev}/T_{max-beat}$ that range between $1/2$ and $3/2$. The Fibonacci sequence $\{1/1, 1/2, 2/3, 3/5, 5/8, \dots\}$ is a subset of the possible rational ratios $T_{min-rev}/T_{max-beat}$.

Fractional or intra-revival structure of Morse vibrators is quite like that of rotor revivals. In Fig. 4(a) is a Morse revival of higher frequency $\omega_e/2\pi c = 42(cm^{-1})$ and more states ($n_{max} = 20$) than the one in Fig. 3(a), but with the same anharmonicity $\omega_x/2\pi c = 1(cm^{-1})$ and revival period: $T_{rev} = 1T_{min-rev} = 1T_{max-beat} = 1/(2c(cm)^{-1}) \approx 16.7(pico-second)$.

Fractional revival structure is visible as a series of dips on top of Fig. 4(a) and in Fourier amplitude frequency ω_n sum or autocorrelation $A(t)$ spectra [25] in Fig. 4(b).

$$A(t) = \sum_{n=0}^{n_{max}} e^{-i\frac{E_n t}{\hbar}} = \sum_{n=0}^{n_{max}} e^{-i\omega_n t} \quad (14)$$

$|A(t)|$ spectra match Farey-sum sequence used in 1815 by geologist John Farey [9][28] to analyze tidal beats.

A Farey sequence, starting with fraction $0/1$ and ending with fraction $1/1$, builds hierarchies of irreducible rational fractions on a real line between 0.0 and 1.0 [28].

A Farey-sum $\frac{a}{b} + \frac{c}{d} = \frac{a+c}{b+d}$ is a curious process to locate significant fractions $\frac{n}{d}$ between $\frac{a}{b}$ and $\frac{c}{d}$ or overtone ($n : d$) resonances in between an ($a : b$) and a ($c : d$) resonance.

In 1938, Leslie Ford [14] found a geometric description that helps elucidate Farey-sums. Ford geometry views each fraction as a vector and the Farey sum as a vector sum in Denominator(y)-vs-Numerator(x) space such as is plotted for $0 \leq (x, y) \leq 1$ in Fig. 5. A fraction $\frac{a}{b}$ is drawn as a vector with tail at origin and head at the point $(x = a, y = b)$ as shown by examples $\mathbf{V}_{\frac{0}{1}}$ and $\mathbf{V}_{\frac{1}{1}}$, the black and red arrows in Fig. 5 (lower left).

$$\mathbf{V}_{\frac{0}{1}} + \mathbf{V}_{\frac{1}{1}} = \begin{pmatrix} 0 \\ 1 \end{pmatrix} + \begin{pmatrix} 1 \\ 1 \end{pmatrix} = \begin{pmatrix} 1 \\ 2 \end{pmatrix} = \mathbf{V}_{\frac{1}{2}} \quad (15a)$$

The green arrow in Fig. 5 is $\mathbf{V}_{\frac{1}{2}}$. Each vector $\mathbf{V}_{\frac{n}{d}}$ points to or intersects a real value $x = n/d$ on the top ($y = 1$)-line of Fig. 5. Ford [14] discovered that each $x = n/d$ is a tangent point for a circle having diameter $1/d^2$ hanging below the top ($y = 1$)-line that is itself tangent to infinite sequences of smaller such circles, each tangent to the next and converging on $x = n/d$. The ($d = 1$)-Ford-circle is a unit-diameter circle sliced to fit the unit (x, y) -area with a pair of tangent semi circles belonging to unit Ford base vectors $\mathbf{V}_{\frac{0}{1}}$ and $\mathbf{V}_{\frac{1}{1}}$. Fractions $\frac{0}{1}$ and $\frac{1}{1}$ make a second ($d=2$)-Ford circle of diameter $1/2^2$ in the upper center of Fig. 5 pointed out by sum $\mathbf{V}_{\frac{1}{2}} = \mathbf{V}_{\frac{0}{1}} + \mathbf{V}_{\frac{1}{1}}$ in Eq. (15a).

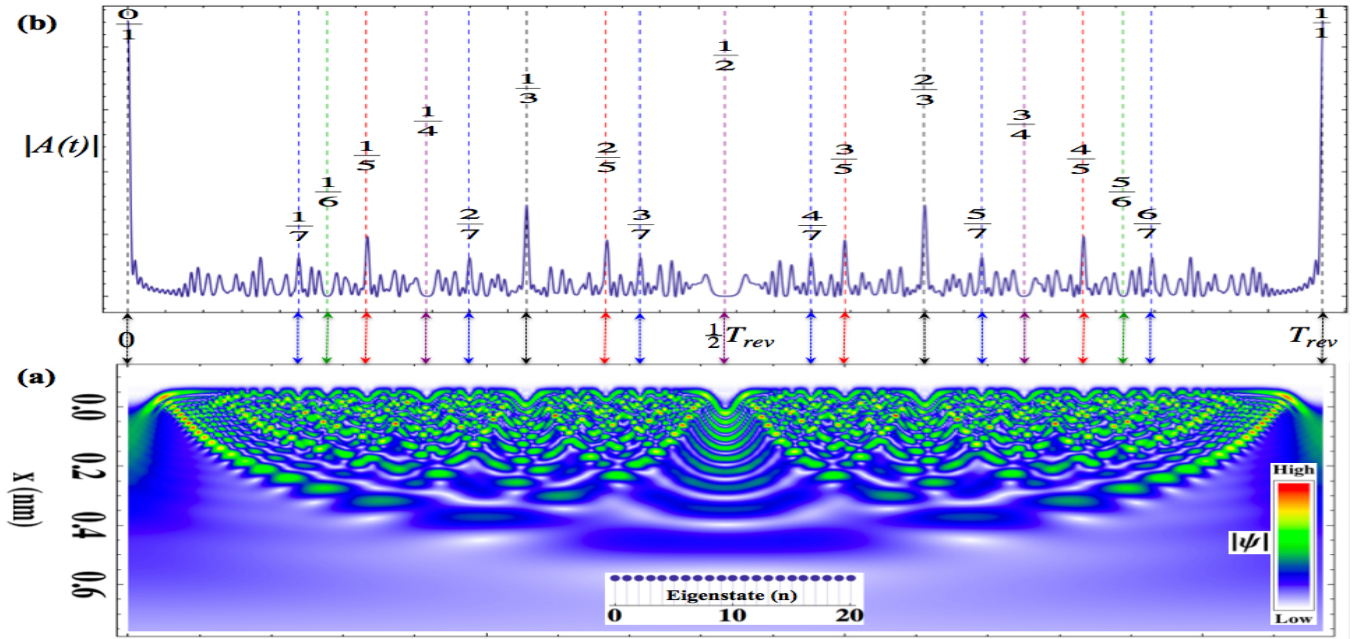


FIG. 4. The Farey-sum sequence structure appears in Morse oscillator space-time pattern for $w_e/2\pi c = 42(\text{cm}^{-1})$ and $w_\chi/2\pi c = 1(\text{cm}^{-1})$ with $n_{max} = 20$. (a) One complete revival period plot of the wave packet has color denote magnitude $|\Psi(x,t)|$. (b) The norm of autocorrelation function ($|A(t)|$) with $n_{max} = 20$ is plotted in one complete revival period T_{rev} whose fractions $\{\frac{0}{1}, \frac{1}{7}, \frac{1}{6}, \frac{1}{5}, \frac{1}{4}, \frac{2}{7}, \frac{1}{3}, \frac{2}{5}, \frac{3}{7}, \frac{1}{2}, \frac{4}{7}, \frac{3}{5}, \frac{2}{3}, \frac{5}{7}, \frac{3}{4}, \frac{4}{5}, \frac{5}{6}, \frac{6}{7}, \frac{1}{1}\}$ are denoted by the vertical dashed lines. The double arrows connecting (a)-(b) indicate the corresponding time events having peaks (or nodes) for time fraction $\frac{n}{d}$ of odd (or even) depth d .

It is tangent to “parent” Ford circles for $\frac{0}{1}$ and $\frac{1}{1}$. Also shown is $(d=3)$ -Ford circle for vector $\mathbf{V}_{\frac{1}{3}} = \mathbf{V}_{\frac{0}{1}} + \mathbf{V}_{\frac{1}{2}}$ that is tangent to circles of its parent fractions $\frac{0}{1}$ and $\frac{1}{2}$.

$$\mathbf{V}_{\frac{0}{1}} + \mathbf{V}_{\frac{1}{2}} = \begin{pmatrix} 0 \\ 1 \end{pmatrix} + \begin{pmatrix} 1 \\ 2 \end{pmatrix} = \begin{pmatrix} 1 \\ 3 \end{pmatrix} = \mathbf{V}_{\frac{1}{3}} \quad (15b)$$

Thales 600-BCE rectangle-in-circle geometry is sufficient to derive Ford geometry. Tangent Ford circles like the $\frac{0}{1}$, $\frac{1}{1}$, and $\frac{1}{2}$ circles in Fig. 5 meet at corners of similar Thales rectangles whose vertical diagonals are circle diameters hanging below their respective fraction points. Circle diameters subtend 90° corners by Thales theorem. The $\frac{0}{1}$ and $\frac{1}{2}$ corners meet where the $\mathbf{V}_{\frac{1}{2}}$ -vector line crosses the $\frac{0}{1}$ -circle. This is the $\frac{0}{1}$ - $\frac{1}{2}$ -circle-tangent point. A $\frac{0}{1}$ -diameter line through that point intersects the vertical diameter of the $\frac{1}{2}$ -circle at its center thus defining it. Similar geometry (not drawn) applies to the $\frac{1}{2}$ - $\frac{1}{1}$ -circle-tangent. A Farey-sum of a circle-tangent pair is a new Ford circle and fraction as shown by examples $\frac{0}{1} + \frac{1}{2} = \frac{1}{3}$ in Eq. (15b) or $\frac{1}{2} + \frac{1}{1} = \frac{2}{3}$ listed in level-3 of the Farey-sum-tree on the righthand side of Fig. 5. Farey sums that give reducible fractions $\frac{N}{D} = \frac{n \cdot f}{d \cdot f}$ are labeled by their reduced form $\frac{n}{d}$ with the shortest allowed Ford vector, least depth or denominator d , and largest possible Ford circle.

Continued Farey-sums of Ford vectors give sequences of circles each belonging to an irreducible fraction $\frac{n}{d}$ and its vector $\mathbf{V}_{\frac{n}{d}}$. In Fig. 5, these circles nest in the

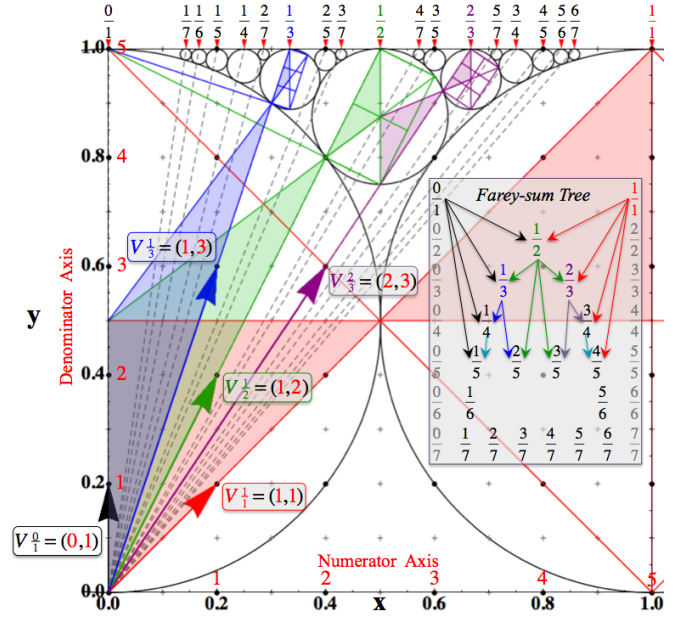


FIG. 5. Ford circles and vectors with Farey-sum sequence.

area between their original Farey “grandparent” circles $\mathbf{V}_{\frac{0}{1}}$ and $\mathbf{V}_{\frac{1}{1}}$. A Farey-sum-tree of fractions of depth $d \leq 7$ $\{\frac{0}{1}, \frac{1}{7}, \frac{1}{6}, \frac{1}{5}, \frac{1}{4}, \frac{2}{7}, \frac{1}{3}, \frac{2}{5}, \frac{3}{7}, \frac{1}{2}, \frac{4}{7}, \frac{3}{5}, \frac{2}{3}, \frac{5}{7}, \frac{3}{4}, \frac{4}{5}, \frac{5}{6}, \frac{6}{7}, \frac{1}{1}\}$ is shown in box on the right of Fig. 5 and represented by a total of 19 sequentially and mutually tangent circles.

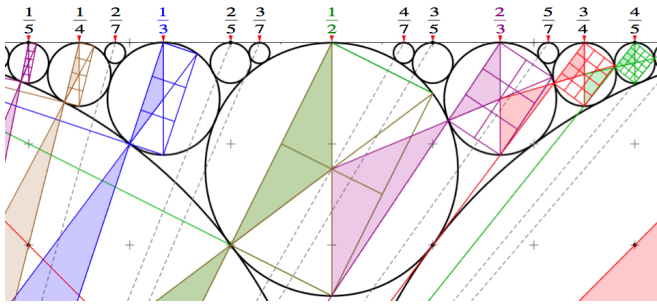


FIG. 6. “Quantization” inside Ford circles: pixel lattices of $\{(1 \times 5), (1 \times 4), (1 \times 3), (1 \times 2), (2 \times 3), (3 \times 4), (4 \times 5)\}$ rectangles lie circumscribed by circles of fractions $\{\frac{1}{5}, \frac{1}{4}, \frac{1}{3}, \frac{1}{2}, \frac{2}{3}, \frac{3}{4}, \frac{4}{5}\}$.

A revealing portrait emerges of quantum “fractal” structure filling the area below the top line with ever tinier $\frac{1}{d^2}$ -diameter circles as spectral depth d increases.

By construction all Ford-vector and Thales-rectangle slopes are rational, but surprisingly so are their aspect ratios “quantized” into n -by- d pixel arrays. For example, (1×3) , (1×2) , and (2×3) pixel arrays lie inside $\{\frac{1}{3}, \frac{1}{2}, \frac{2}{3}\}$ circles in Fig. 5, and Fig. 6 shows finer $(n \times d)$ arrays of pixel rectangles circumscribed by $\frac{n}{d}$ -circles.

In conclusion, exact Morse oscillator eigensolutions allow more detailed analysis of their quantum dynamics. A key top-level-to-dissociation gap parameter δ_N provides a concise revival time formula in terms of two fundamental periods, a semiclassical $T_{min-rev}$ found by Wang and Heller and a longest quantum beat period $T_{max-beat}$. This shows that complete revival periods may be composed of integer numbers of the two. Finally, fractional revivals seen in rotor pulse evolution is also shown to be present in Morse wave dynamics in the form of Farey-sum spectral sub-structure. A Ford-circles geometry relating rational fractions to real numbers may be developed to visualize these phenomena and may eventually have application to quantum information processing and computing.

* alvali@uark.edu

† wharter@uark.edu

- [1] J. H. Eberly, N. B. Narozhny, and J. J. Sanchez-Mondragon, Phys. Rev. Lett. **44**, 1323 (1980).
- [2] E. J. Heller, J. Chem. Phys. **62**, 1544 (1975).
- [3] R. S. McDowell, C. W. Patterson, and W. G. Harter, Los Alamos Science **3**, 38 (1982).
- [4] A. H. Zewail, Science **242**, 1645 (1988).
- [5] B. Feuerstein and U. Thumm, Phys. Rev. A **67** (2003).
- [6] A. Rudenko, T. Ergler, B. Feuerstein, K. Zrost, C. D. Schroter, R. Moshhammer, and J. Ullrich, Chem. Phys. **329**, 193 (2006).
- [7] T. Niederhausen and U. Thumm, Phys. Rev. A **77** (2008).
- [8] K. Ohmori, Annu. Rev. Phys. Chem. **60**, 487 (2009).
- [9] J. Farey, Philos. Mag. **47**, 385 (1816).
- [10] W. G. Harter, Phys. Rev. A **64** (2001).
- [11] W. G. Harter, J. Mol. Spectrosc. **210**, 166 (2001).
- [12] H. Mack, M. Bienert, F. Haug, M. Freyberger, and W. Schleich, phys. stat. sol. (b) **233**, 408 (2002).
- [13] M. Gilowski, T. Wendrich, T. Müller, C. Jentsch, W. Ertmer, E. M. Rasel, and W. P. Schleich, Phys. Rev. Lett. **100** (2008).
- [14] L. R. Ford, The American Mathematical Monthly **45**, 586 (1938).
- [15] A. Z. Li, *Quantum Resonant Beats and Revivals in the Morse Oscillators and Rotors*, Ph.D. thesis, University of Arkansas (2013).
- [16] P. M. Morse, Phys. Rev. **34**, 57 (1929).
- [17] V. P. Gutschick and M. M. Nieto, Phys. Rev. D **22**, 403 (1980).
- [18] J. P. Dahl and M. Springborg, J. Chem. Phys. **88**, 4535 (1988).
- [19] S. Kais and R. D. Levine, Phys. Rev. A **41**, 2301 (1990).
- [20] M. Angelova and V. Hussin, J. Phys. A: Math. Theor. **41** (2008).
- [21] Z. Wang and E. J. Heller, J. Phys. A: Math. Theor. **42** (2009).
- [22] A. B. McCoy, Chem. Phys. Lett. **501**, 603 (2011).
- [23] S. Dong, R. Lemus, and A. Frank, Int. J. Quantum Chem. **86**, 433 (2002).
- [24] I. S. Averbukh and N. F. Perelman, Phys. Lett. A **139**, 449 (1989).
- [25] R. W. Robinett, Phys. Rep. **392**, 1 (2004).
- [26] T. Lohmuller, V. Engel, J. Beswick, and C. Meier, J. Chem. Phys. **120**, 10442 (2004).
- [27] V. V. Eryomin, S. I. Vetchinkin, and I. M. Umanskii, J. Chem. Phys. **101**, 10730 (1994).
- [28] G. H. Hardy and E. M. Wright, *An Introduction to the Theory of Numbers*, 5th ed. (Oxford University Press, New York, 1979).